Structural and optical studies of local disorder sensitivity in natural organic–inorganic self-assembled semiconductors

2009 J. Phys. D: Appl. Phys. 42 185405

(http://iopscience.iop.org/0022-3727/42/18/185405)

IOP PUBLISHING JOURNAL OF PHYSICS D: APPLIED PHYSICS

J. Phys. D: Appl. Phys. **42** (2009) 185405 (7pp) doi:10.1088/0022-3727/42/18/185405

Structural and optical studies of local disorder sensitivity in natural organic–inorganic self-assembled semiconductors

G Vijaya Prakash[1,5], K Pradeesh[1], R Ratnani[2], K Saraswat[2], M E Light[3] and J J Baumberg[4]

[1] Nanophotonics Lab, Department of Physics, Indian Institute of Technology Delhi, New Delhi, India
[2] Department of Pure and Applied Chemistry, MDS University, Ajmer, India
[3] School of Chemistry, University of Southampton, Southampton, UK
[4] Nanophotonic Centre, Cavendish Laboratory, University Cambridge, Cambridge CB3 OHE, UK

E-mail: prakash@physics.iitd.ac.in

Received 19 January 2009, in final form 10 June 2009
Published 28 August 2009
Online at stacks.iop.org/JPhysD/42/185405

Abstract

The structural and optical spectra of two related lead iodide (PbI) based self-assembled hybrid organic–inorganic semiconductors are compared. During the synthesis, depending on the bridging of organic moiety intercalated between the PbI two-dimensional planes, different crystal structures are produced. These entirely different networks show different structural and optical features, including excitonic bandgaps. In particular, the modified organic environment of the excitons is sensitive to the local disorder both in single crystal and thin film forms. Such information is vital for incorporating these semiconductors into photonic device architectures.

(Some figures in this article are in colour only in the electronic version)

1. Introduction

Organic–inorganic hybrid nanostructures have recently emerged as highly promising systems for applications as optoelectronic devices, also opening up new dimensions to nanotechnology [1, 2]. Among these, self-organized systems based on the large family of layered perovskites have attracted attention because of their unique crystal structures and functional physical and optical properties. They are self-organized low-dimensional crystals derived from component 3D networks of AMX_3 type perovskite, where A is an organic moiety, M is a divalent metal (such as Pb^{2+} and Sn^{2+}) and X is a halide (such as I, Br and Cl). More recent crystal engineering strategies involve reducing the higher-dimensional parent structures into zero-, one-, two- or three-dimensional hybrid networks [3–6]. The simplest 2D layered hybrids consist of MX_4^2 corner-sharing metal halide octahedra separated by mono- or bi-layers of organic moiety. Self-assembling organic moieties with the parent 3D networks access a great variety of new crystal structures [7]. These layered hybrids have been considered as *natural semiconductor multiple quantum wells* and show strong room-temperature excitonic optical features with large exciton binding energy and oscillator strength due to the low dimensionality of the inorganic structure. The large dielectric mismatch, between the organic and the inorganic layers, provides additional dielectric confinement which greatly influences the physical and optical properties [8]. Though not completely understood, the exciton properties are strongly influenced by the dielectric mismatch and also the structural arrangement of the inorganic layers.

Low-dimensional lead iodide based hybrid perovskites are of particular current interest due to their structural, magnetic, optical nonlinear and optoelectronic functionality [9–11]. These hybrids thermally stable up to $\sim$150 °C and show large exciton binding energies (>220 meV) and excitons are observable even at room temperature [12, 13]. Therefore, they

[5] Author to whom any correspondence should be addressed.

are considered to be a more suitable alternative to organic semiconductors, such as J-aggregates, for optoelectronic applications such as strong coupling and 1D gratings [10–16]. Although the structure and the optical studies of lead halide based perovskite type hybrids are fairly well understood [9–11, 17–19], the correlation between the film-processing and the optical properties are not completely understood.

Here we present synthesis, crystal structure and optical characteristics of two different low-dimensional materials produced by incorporating aniline-based organic moieties into the well-known parent PbI 3D network. When chloro-aniline is substituted as the organic moiety, the organic–inorganic hybrid assembles as a 2D layered network, wherein two chloroanilines are intercalated and bridged between the two-dimensional PbI planes. On the other hand, for methoxy-aniline the resultant network is composed of 1D PbI ribbons. We present the structural and optical properties of thin film as well as single crystals, which exhibit strong excitonic absorption and photoluminescence. We have further investigated the morphological dependence of the optical properties, influenced by their lattice interactions.

2. Experimental

Stoichiometric quantities of organic moiety (4-X-$C_6H_4NH_2$, where X = Cl or CH_3O) and PbI_2 (from Aldrich Chemicals) were used without any further purification. The molar ratio between the organic and PbI_2 was maintained at 2 : 1. The organic moiety is dissolved in aqueous hydroiodic acid (HI 55%) in the presence of anhydrous ethanol. A solution of PbI_2 in concentrated aqueous HI was then added to the organic solution gradually with stirring at 60 °C. The resulting solution was allowed to rest at 60 °C for 4 h and then cooled slowly (5 °C h^{-1}) to room temperature without stirring. The precipitate was filtered off and dried. Large single crystals were harvested from the saturated methanolic solutions of the respective compounds. Single-crystal x-ray diffraction [19] studies reveal the chemical formulae as (a) $(Cl\text{-}C_6H_4NH_3)_2PbI_4$ (hereafter CAPI) and (b) $(CH_3O\text{-}C_6H_4NH_3)_2Pb_3I_8 \cdot 2H_2O$ (hereafter MOAPI) for the respective compounds. Thin films were obtained by spin-coating acetonitrile solutions of the respective compounds onto a glass substrate. For thick films, a solution of each respective compound is either drop-cast onto a glass substrate or concentrated through solvent evaporation before spinning at different rates. Single crystal x-ray diffraction and glancing angle x-ray diffraction (GAXRD) were carried out for the single crystals and thin films, respectively. Thermo-gravimetry (TG) and differential thermo-gravimetry (DTG) were carried out between 30 and 800 °C at a scan rate of 5 °C min^{-1} in a N_2 atmosphere. UV–visible absorption spectra were taken for the spin-coated films. Photoluminescence (PL) was recorded by pumping the spin-coated films using 337 nm excitation from a pulsed N_2 laser and dispersed into a monochromator attached to a cooled CCD. Single crystal emission images and spectra were taken through a high-resolution microscope coupled to a monochromator, by back-illuminating with the 337 nm N_2 laser.

3. Results and discussion

3.1. Crystal structure

Both the crystal structures [27][6] are studied in detail here, and we resolve their full atomic arrangement. The compound CAPI crystallizes in the monoclinic space group $P2_{1/c}$ in which the asymmetric unit consists of half a $(PbI_4)^{2-}$ anion and one $(Cl\text{-}C_6H_4NH_3)^+$ cation. The structure comprises well-ordered organic and inorganic layers, arranged alternately. They are stacked along the a-(1 0 0) direction with layers infinitely extended in the bc plane (figure 1(*a*)). There are two types of iodine (I) atoms defined by their different connectivities: terminal, I(1), and double bridging, I(2), iodine atoms. Six iodine atoms are bonded to lead (Pb) atoms to form an octahedron with Pb at the centre and I at the corners. The Pb–I distance varies from 3.167 to 3.211 Å. The *trans* Pb–I bond angle is 180° and the *cis* Pb–I bond angle varies from 86.81° to 93.12°. The Pb–I–Pb bond angle is 143.01°. The Pb–I–Pb bond angle indicates that the corner sharing of PbI_6 octahedra is distorted. This distortion is both an in-plane (away from the ideal square grid) distortion as well as a correlated out-of-plane distortion.

In contrast, MOAPI crystallizes in the monoclinic space group $P2_1$ with the asymmetric unit consisting of a $(Pb_3I_8)^{2-}$ anion, two $(CH_3O\text{-}C_6H_4NH_3)^+$ cations and two water molecules (figure 1(*b*)). The crystal structure of MOAPI features triple chains of edge-shared PbI_6 octahedra forming ribbons. Based on the connectivity of the iodine atoms to the Pb atoms (defined similarly to CAPI), there are now three types of iodine atoms: terminal, I(1), I(8), double bridging, I(2), I(7), and triple-bridging atoms, I(3), I(4), I(5), I(6). Considering the location as well as the connectivity of the Pb atoms gives two types: the ones in the middle of the chain, Pb(2), which are entirely bonded to triple-bridging iodine atoms and the others at the side of the chain, Pb(1), Pb(3), which are bonded to all three types of iodine atoms. The chain extends along the a direction in a herringbone fashion parallel to (0 1 1) and (0 1 $\bar{1}$) via edge-sharing of PbI_6 octahedra. The shortest Pb–I distance is 3.024 Å (between a side Pb atom and a terminal iodine atom) and the largest is 3.423 Å (between a side Pb atom and a triple-bridging iodine atom). The *trans* Pb–I bond angle varies between 170.69° and 179.49° and the *cis* Pb–I bond angle varies between 84.72° and 94.64°. Hence there are rather complex differences in the orientation of the PbI components induced by the simple change in the organic spacer molecule.

[6] Cell dimensions and intensity data were recorded at 120 K, using a Bruker Nonius KappaCCD area detector diffractometer mounted at the window of a rotating Mo anode (λ (Mo Kα) = 0.710 73 Å). The crystal-to-detector distance was 30 mm and ϕ and Ω scans were carried out to fill the asymmetric unit. Data collection and processing were carried out using the programs COLLECT (data collection software, Nonius B.V., 1998.), and DENZO. An empirical absorption correction was applied using SADABS (Sheldrick, G M SADABS—Bruker Nonius area detector scaling and absorption correction—V2.10). The structures were solved via direct methods and refined by full matrix least squares (SHELX97: Programs for Crystal Structure Analysis (Release 97-2). G M Sheldrick, Institüt für Anorganische Chemie der Universität, Tammanstrasse 4, D-3400 Göttingen, Germany, 1998) on F^2. Non-hydrogen atoms were refined anisotropically and hydrogen atoms were treated using a riding model. MOAPI was refined as racemic twin.

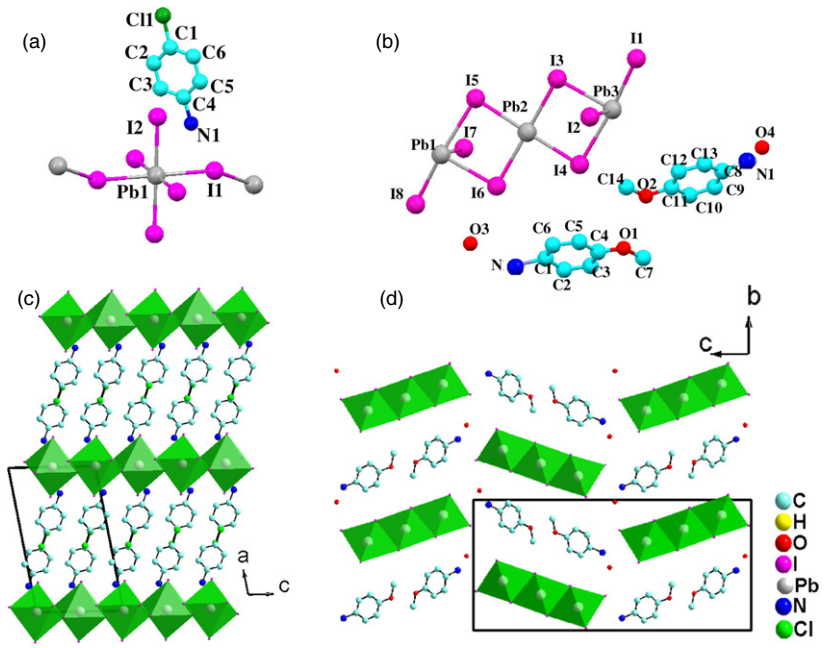

Figure 1. (*a*) and (*b*) are crystal structures of CAPI and MOAPI with the asymmetric unit labelled, respectively. Thermal ellipsoids are drawn at 50% probability level. (*c*) Layered structure of CAPI viewed along the *b* direction and (*d*) MOAPI packing diagram when viewed along the *a* direction. The unit cell edges are shown with solid lines. Here the arrangement of spin-coated organic–inorganic perovskites on the substrate are aligned along the (1 0 0) plane for CAPI and along the (0 1 1) plane for MOAPI. All the hydrogen atoms of organic molecules are omitted for clarity.

Although in both CAPI and MOAPI a layering arrangement persists, they are entirely different from each other. In general, these hybrids are formed by the intercalation of appropriately sized guest moieties into the empty spaces within PbI_2 crystalline host. However, the dimensionality of the crystalline formation is typically dependent on the nature and shape of the guest moiety [17]. In CAPI edge-shared PbI_6 octahedra form a 2D layered structure with the organic acting as spacers in between each layer with (1 0 0) spacing of 15.08 Å (figure 1(*c*)). On the other hand, MOAPI, as viewed along the *a* (1 0 0) direction (figure 1(*d*)), is seen as a corrugated layered arrangement. In CAPI, two organic cations $(Cl\text{-}C_6H_4NH_3)^+$ are aligned almost opposite to each other and are approximately bonded perpendicular to the inorganic layered network through their hydrogen bonding of their respective amino groups. This contrasts with MOAPI where although two organic cations $(CH_3O\text{-}C_6H_4NH_3)^+$ are aligned opposite to each other, they are almost in-line with the PbI ribbon, and the PbI ribbons of nearby layers are distorted from the (0 1 1) plane by the accommodation of water molecules. This type of trapping of water molecules between PbI network and cations has indeed been observed previously [19].

Summarizing, the CAPI PbI network is multi-layered with a layer separation of 6.33 Å and infinitely extended in sheets, whereas MOAPI is built of ribbons of dimensions 13.78 × 6.44 Å extended infinitely along the *a* direction (figure 1). The complete details of the crystallographic data are given in table 1.

3.2. Physical properties

The GAXRD of spin-coated thin films of CAPI and MOAPI is illustrated in figure 2(*a*). Labels I and II indicate the films of thin (thickness ∼40–120 nm) and thick (>150 nm) spin-coated films, respectively. The presence of strong peaks from (1 0 0) and (2 0 0) for CAPI (I) confirms that the 'layered perovskite sheets' are aligned normal to the (1 0 0) plane, indicating the preferred orientation on the glass substrate. Similarly, the strong (0 1 1) peak in MOAPI (I) implies that the perovskites are layered along this corresponding plane. The corresponding *d* spacings are 15.08 Å and 12.57 Å for CAPI and MOAPI thin films, respectively, and are the same as observed from the single-crystal diffraction analysis. We note that complete layering is critically dependent on the thickness of the film and the solvent used. As an example, we have also included XRD of thicker films (CAPI(II) and MOAPI(II)), wherein the appearance of other diffraction peaks clearly indicates that the layered structure has been completely disordered. Further, note that the film formation is solvent critical: thin films made out of acetonitrile as solvent show more uniformity in film formation, while for methanol the films re-crystallize into micro-needles. In general, the structural arrangement and the mechanical strengths of these layered perovskites are strongly dependent on ordering and Pb–I bonding of PbI stacks, and how the organic moiety has been linked in between the layers through the ammonium headgroup.

The TG and DTG curves of CAPI (figure 2(*b*)) suggest that these hybrid structures are quite stable up to temperatures of 220–230 °C. In CAPI, below 222.8 °C, the organic intermediate is stable and as the temperature increases further, a weight loss of about 52% (2.422 mg of 4.648 mg) is observed. This suggests that the organic (as well as HI) is decomposed and PbI_2 remains. In MOAPI (figure 2(*c*)), the water molecules which were trapped in between the PbI ribbons and the organic molecules decompose at around 64.8 °C, indicating that the

Table 1. Crystallographic data of CAPI and MOAPI.

Crystal data	CAPI	MOAPI
Empirical formula	$C_{12}H_{14}Cl_2I_4N_2Pb$ or $2[Cl\text{-}C_6H_4NH_3]^+$, $[PbI_4]^{2-}$	$C_{14}H_{24}I_8N_2O_4Pb_3$ or $2[CH_3O\text{-}C_6H_4NH_3]^+$, $[Pb_3,I_8]^{2-}$ $2(H_2O)$
Formula weight	971.94 (g mol^{-1})	1921.12 (g mol^{-1})
Temperature	120(2) K	120(2) K
Wavelength	0.710 73 Å	0.710 73 Å
Crystal system	Monoclinic	Monoclinic
Space group	$P2_1/c$	$P2_1$
Unit cell dimensions	$a = 15.3120(3)$ Å $b = 8.103\,40(10)$ Å $\beta = 99.8320(10)^\circ$ $c = 9.0347(2)$ Å	$a = 4.4674(2)$ Å $b = 13.6450(8)$ Å $\beta = 94.296(2)^\circ$ $c = 29.0326(16)$ Å
Volume	1104.55(4) Å^3	1764.79(16) Å^3
Z	2	2
Density (calculated)	2.922 mg m^{-3}	3.615 mg m^{-3}
Crystal	Fragment; yellow	Needle; pale yellow
Crystal size	$0.2 \times 0.08 \times 0.02$ mm^3	$0.08 \times 0.01 \times 0.01$ mm^3
Data collection		
Absorption coefficient	13.465 mm^{-1}	21.293 mm^{-1}
$F(0\,0\,0)$	856	1648
θ range for data collection	3.40–27.48°	2.99–27.48°
Index ranges	$-91 \leqslant \eta \leqslant 91$, $-9 \leqslant \kappa \leqslant 01$, $-11 \leqslant \lambda \leqslant 11$	$-5 \leqslant \eta \leqslant 5$, $-71 \leqslant \kappa \leqslant 71$, $-73 \leqslant \lambda \leqslant 73$
Reflections collected	13 065	17 811
Independent reflections	2529 [$R_{int} = 0.0404$]	7209 [$R_{int} = 0.0373$]
Completeness to $\theta = 27.48^\circ$	99.80%	99.40%
Absorption correction	Semiempirical from equivalents	Semiempirical from equivalents
Max. and min. transmission	0.7645 and 0.1537	0.8153 and 0.2807
Refinement method	Full-matrix least-squares on F^2	Full-matrix least-squares on F^2
Data/restraints/parameters	2529/0/98	7209/164/297
Goodness-of-fit on F^2	1.142	1.095
Final R indices [$F^2 > 2\sigma(F^2)$]	$R1 = 0.0254$, $wR2 = 0.0613$	$R1 = 0.0359$, $wR2 = 0.0741$
R indices (all data)	$R1 = 0.0272$, $wR2 = 0.0622$	$R1 = 0.0423$, $wR2 = 0.0777$
Largest diff. peak and hole	0.867 and -2.270 e Å^{-3}	1.132 and 1.190 e Å^{-3}

binding interaction of water in the crystal is relatively low, with a weight loss of 1.56% which is almost equal to the calculated weight per cent of water molecules (1.77%). The organic within the PbI chains is stable up to temperatures around 235 °C. The decomposition temperature is higher for MOAPI compared with that of CAPI, probably due to the strong binding with the inorganic components in this crystal structure. The decomposition of CAPI and MOAPI occurs as follows:

$$\mathrm{CAPI}: (\mathrm{Cl}-\mathrm{C_6H_4NH_3})_2\mathrm{PbI_4}(100\%) \rightarrow \mathrm{PbI_2}(47.42\%) + 2\mathrm{ClC_6H_4NH_2}(26.25\%) + \mathrm{HI}(26.31\%),$$

$$\mathrm{MOAPI}: (\mathrm{CH_3O}-\mathrm{C_6H_4NH_3})_2\mathrm{Pb_3I_8}\cdot 2(\mathrm{H_2O})100\%) \rightarrow 3\mathrm{PbI_2}(68.13\%) + 2\mathrm{CH_3OC_6H_4NH_2}(12.13\%) + \mathrm{HI}(12.56\%) + \mathrm{H_2O}(1.77\%).$$

3.3. Optical properties

The optical properties of excitons in these hybrids are of much interest because of their strength and resonant behaviour. Apart from the usual quantum confinement, the large variation in dielectric constant between barrier (organic) and quantum well (PbI) play a vital role [24]. Though structure and optical studies of similar hybrids were extensively studied earlier [9–11, 17], the effects of layered formation and their defects on optical properties are not completely understood. In this case, we focus on the formation and thin film and the effect of thickness and crystallinity on the optical features. Figures 3(*a*) and 3(*b*) represent room-temperature absorption and photoluminescence (PL) of CAPI and MOAPI. The room-temperature absorption of CAPI and MOAPI shows two principal absorption lines: a broad absorption at ∼400 nm and a strong narrow peak at ∼480 nm (figure 3(*a*)). While the former is attributed to the charge transfer transition between the organic and inorganic layers, the narrow absorption peak at about 480 nm is attributed to the lowest exciton within the inorganic layers [22]. Both of these hybrid structures give a narrow exciton spectral line shape with spectral widths <20 nm.

Both CAPI and MOAPI thin films show bright greenish room-temperature photoluminescence (PL) upon UV excitation (at 337 nm). The primary origin of PL from both these hybrid structures is related to the lowest exciton (figure 3(*b*)), giving PL spectra with narrow spectral peaks (width ∼19 nm) which are slightly asymmetric. As compared with CAPI, MOAPI shows a red shift in both absorption as well as PL peak emission. Although both these hybrids are structurally different (one is 2D layered, while the other is of 1D ribbon type), the red shift could be understood as an

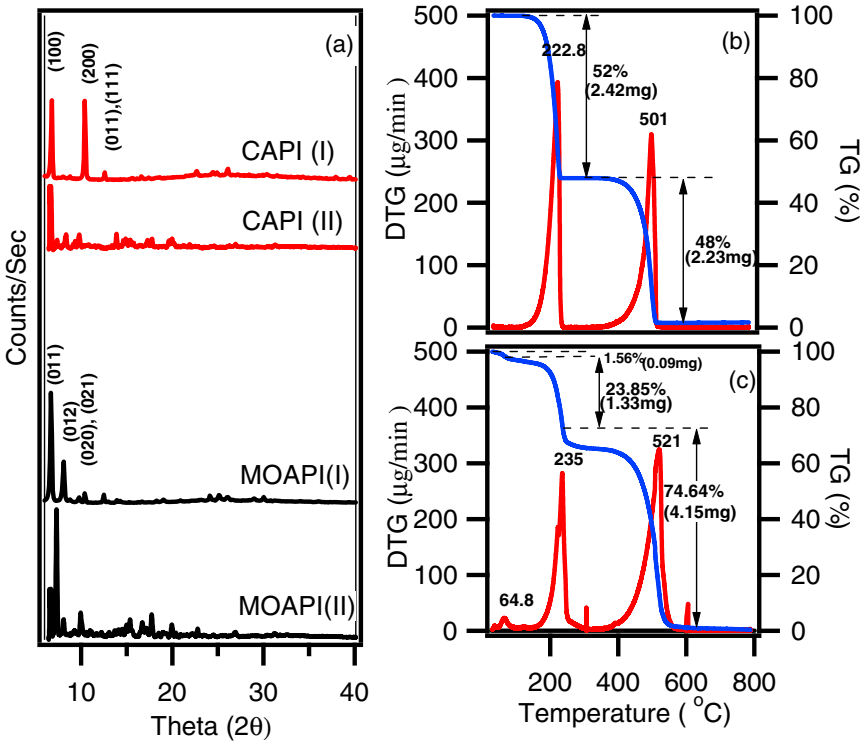

Figure 2. (*a*) GAXRD of CAPI and MOAPI films. I and II denote the data for thin and thick films, respectively (see text). (*b*) and (*c*) DTG (red) and TG (blue) curves of CAPI and MOAPI, respectively. (Colour online.)

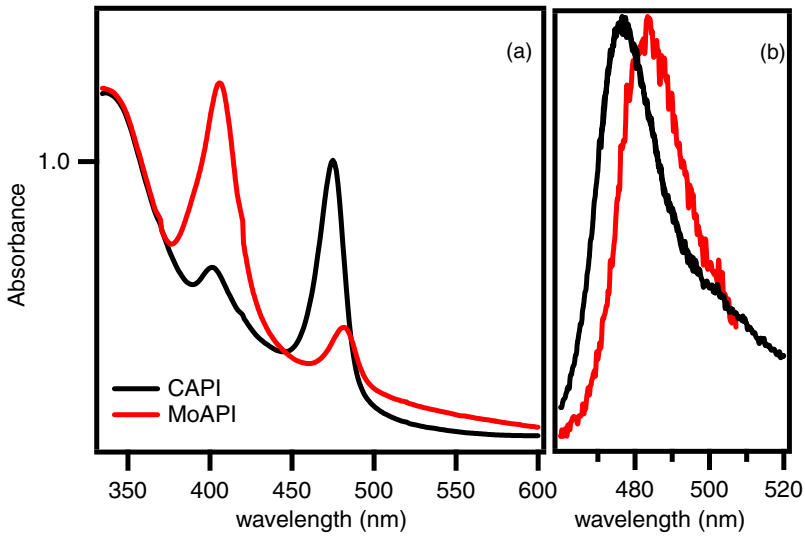

Figure 3. (*a*) Absorption spectra of CAPI and MOAPI spin-coated films. (*b*) Photoluminescence of CAPI (black) and MOAPI (red). (Colour online.)

effect of so-called 'dielectric confinement' due to the additional low dielectric organic layers surrounding the excitonic PbI sites rather than conventional quantum confinement effects. However, other studies, such as theoretical modelling, are further needed to account for the Coulomb interaction in these complex carrier environments [18].

Our extensive study shows that the exciton absorption peak position and relative absorption are strongly dependent on thickness and the solvent from which the films were spin-coated. For uniform thin films of CAPI between ∼40 and 120 nm thick, exciton absorption is always strong and remains at 40% dominating the absorption of charge-transfer band (∼400 nm); however, in thicker films, the absorption strength of charge-transfer peak (∼400 nm) is dominant over the exciton absorption. This could be possibly due to the alignment of ordered (1 0 0) layers which gets disturbed after a certain critical film thickness. These observations are also supported by XRD analysis, as mentioned previously (figure 2(*a*)). We have experimentally verified that controlled spin-coating of films of thickness ranging between 40 and 120 nm is optimum to observe strong exciton absorption. On the other hand, in the case of MOAPI, the PbI ribbons are surrounded by the organic

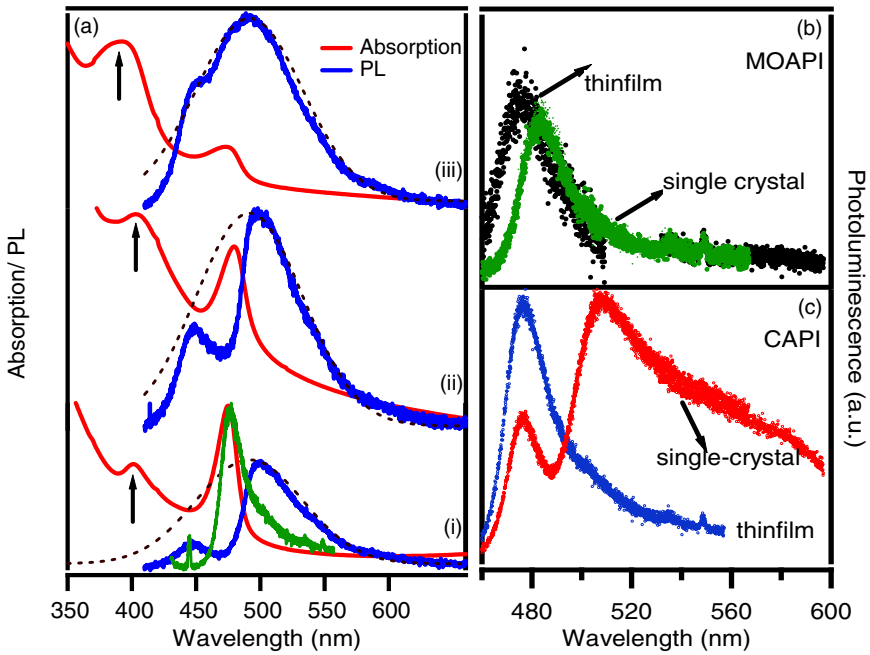

Figure 4. (*a*) Absorption (red) and photoluminescence (PL) (blue) for various thicknesses of spin-coated CAPI films (see text). Spectra are shifted along the *y*-axis for clarity. PL of optimized thickness (∼120 nm) film is also shown in green colour for comparison. The dotted line is a Gaussian envelope drawn as a guide to the eye. Room-temperature photoluminescence of single crystals and optimized thin film of (*b*) MOAPI and (*c*) CAPI. (Colour online.)

environment and the network appears almost independent of the film thickness as compared with CAPI; the charge-transfer absorption (at ∼400) is more than 40% to that of exciton absorption peak.

The room-temperature photoluminescence measurements provide further evidence of thickness-dependent disorder sensitivity. Figure 4 represents the absorption and photoluminescence of thicker films of CAPI and photoluminescence of CAPI and MOAPI crystals. While films of MOAPI do not show any appreciable difference in absorption/PL features with thickness, CAPI shows a marked difference in optical features with thickness change. Figure 4(*a*) shows both absorption and PL spectra of various thicknesses of CAPI, derived from different spinning rates. Thicknesses estimated from the spinning rates are ∼170, 300 and 450 nm for the respective labels i, ii and iii. As seen from figure 4, as thickness increases the absorption strengths of the charge-transfer related band (at ∼400 nm) are more prominent than exciton related absorption (at ∼480 nm). Also, the corresponding PL is clearly red-shifted with a broad spectrum of about 60–70 nm width, as compared with the PL (of width <20 nm) of orderly layered films. Similarly, photoluminescence experiments are also performed on single crystals using a high-resolution microscope coupled with a UV laser (337 nm). The PL recorded for MOAPI shows a single peak at about 485 nm, characteristic of exciton related, similar to that of the thin film (figure 4(*b*)). However, for CAPI crystals, the PL shows two distinct peaks: one is the characteristic excitonic PL at ∼480 nm and another is a broadband emission centred at 520 nm (figure 4(*c*)). Both normal and PL high-resolution images of CAPI and MOAPI single crystals are shown in figure 5.

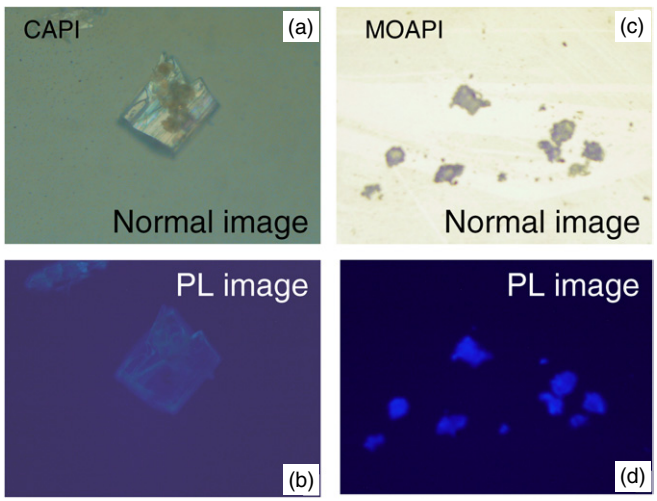

Figure 5. High-resolution normal and photoluminescence (PL) images of CAPI (*a*) and (*b*) and MOAPI (*c*) and (*d*) single crystals. PL images are from confocal microscope arrangement while exciting with 337 nm laser from the bottom of the sample and imaged from the top, using appropriate filters (intensities are not scaled).

Previous studies of similar layered perovskite thin films fabricated by layer-by-layer self assembly [19] reveal that to observe strong exciton related absorption a few layers are enough and charge-transfer absorption (at ∼400 nm) increases linearly with the number of layers, i.e. thickness of the film. Similarly, reports of the well-known layered semiconductor, PbI_2 single crystals made from various methods, show complex PL with a broad red-shifted band as well as the strong lowest exciton peak at ∼494 nm (at $T = 2$ K) [25, 26]. In those extensive studies it is clear that the imperfections in the layer stacking produce additional red-end excitonic

bands due to radiative recombination of the trapped carriers, besides conventional recombination of excitons and self-trapped excitons. It is also known that the structural distortions, such as the width of the PbI layer and the Pb–I–Pb in-plane bonding of perovskite sheets, have a considerable impact on the band gap change and, as a consequence, on the optical properties [18, 21]. For comparison, a well-known hybrid perovskite, PhE-PbI [7, 13, 18] has exciton absorption at 523 nm with structural parameters, of well (PbI) and barrier (organic) widths of 6.38 Å and 8.04 Å, respectively, with Pb–I–Pb in-plane bending of 157.42°. This compares with CAPI, which is similar to phE-PbI but with different organic moiety, where the exciton absorption is blue shifted (∼480 nm) with well and barrier widths of 6.33 Å and 8.75 Å and the Pb–I–Pb in-plane bending is 143.01°. Hence structural re-arrangement/distortions could possibly result in drastic changes in the optical properties.

Therefore, this study suggests that for thicker films (>120 nm) and crystals of CAPI, stacking imperfections could arise due to the strain of the thick film/crystal and as a result uneven crystalline planes, which may behave as quantum wells with different widths. Other possibilities are misaligned organic moieties, distorted Pb–I bondings and broken bonds within the inorganic network. Broadly we can interpret our results as, while the absorption peak at ∼480 nm is due to excitons of ordered perovskite layers, much broader PL originates from both ordered and imperfect lattice stacking of the PbI perovskite layers. Further, it is interesting to note that from figure 4(*a*), the broad PL spectrum appears as if it is sliced into two, on either side of the exciton absorption band. Further, as the thickness increases, the splitting in the PL becomes less pronounced. This observed apparent split in the PL emission could be explained as the distortion-related PL with self-absorption effect due to the strong narrow-band exciton absorption of well-ordered layers. Higher-order multi-exciton effects in these hybrid inorganic–organic layered structures are ruled out since the measurements are carried out at low optical excitation powers [22].

4. Conclusions

In summary, we have examined the structural and optical spectra of two related PbI self-assembled hybrid semiconductors and shown that simply changing the bridging organic moiety results in low-dimensional (1D and 2D) inorganic quantum structures. These different 1D and 2D symmetries result in different optical properties as well as different sensitivities to disorder produced when depositing thin films and/or grown into single crystals. In general, optical and electronic structural features critically depend upon (1) ordering and Pb–I bondings of perovskite layers and (2) organic moiety that has been linked in between the two layers through hydrogen bonding of the ammonium headgroup. Further engineering of the emissive properties of these films is thus in prospect by appropriate design of bridging organics, and thus the adjustment of the PbI environment.

Acknowledgments

One of the authors (GVP) acknowledges the financial support from DST, India. This work is part of the *UK–India Education and Research Initiative* (UKIERI) programme and is partly funded by EPSRC grant EP/C511786/1. The authors thank Dr K Koteswara Rao, Taiwan, for his help in recording DTG/TG data. Finally this paper is dedicated to one of the authors, Dr Raju Ratnani, who died in a recent car accident.

References

[1] Huynh W U, Dittmer J J and Alivisatos A P 2002 *Science* **295** 2425–27
[2] Coe S, Woo W K, Bavandi M and Bulovic V 2002 *Nature* **420** 800–3
[3] Kagan C R, Mitzi D B and Dimitrakopoulos C D 1999 *Science* **286** 945–7
[4] Mitzi D B, Wang S, Field C A, Chess C S and Guloy A M 1997 *Science* **267** 1473–6
[5] Mitzi D B, Field C A, Harrison W T A and Guloy A M 1994 *Natur* e **369** 467–9
[6] Mizi D B, Chondroudis K and Kagan C R 2001 *IBM, J. Res. Dev.* **45** 29–45
[7] Ishihara T and Goto T 1989 *Nonlinear Optics of Organics and Semiconductors* vol 36, ed T Kobayashi (Berlin: Springer) p 72
[8] Hong X, Ishihara T and Nurmikko A V 1992 *Phys. Rev.* B **45** 6961–4
[9] Shimizu M 2005 *Phys. Rev.* B **71** 033316
[10] Symonds C, Bellessa J, Plenetet J C, Brehier A, Arashkov R, Lauret J S and Deleporte E 2007 *Appl. Phys. Lett.* **90** 091107
[11] Guloy A M, Tang Z, Miranda P B and Svdanov V I 2001 *Adv. Mater.* **13** 833
[12] Fluegel B *et al* 2004 *Phys. Rev.* B **70** 205308
[13] Ishihara T 1994 *J. Lumin.* **60&61** 269
[14] Lanty G *et al* 2008 *New J. Phys.* **10** 65007
[15] Cheng Z Y *et al* 2003 *Chem. Phys. Lett.* **376** 481
[16] Sumioka K Nagahama H and Tsutsui T 2001 *Appl. Phys. Lett.* **78** 1328
[17] Ruiz-Hitzky E 2004 *Functional Hybrid Materials* ed P G Romero and C Sanchez (Weinheim: Wiley-VCH) p 15
[18] Muljarov E A *et al* 1995 *Phys. Rev.* B **51** 14370
[19] Matsui T *et al* 2002, *Chem. Commun.* 1094
[20] Louvain N *et al* 2007 *Dalton Trans.* 965–70
[21] Knutson J L, Martin J D and Mitzi D B 2005 *Inorg. Chem.* **44** 4699–705
[22] Shimizu M *et al* 2004 *Phys. Rev.* B **69** 15520
[23] Finlayson C E, Vijaya Prakash G and Baumberg J J 2005 *Appl. Phys. Lett.* **86** 041110
[24] Ishihara T, Takahashi J and Goto T 1990 *Phys. Rev.* B **42** 11099–107
[25] Watanabe M, Hayashi T and Kato R 1990 *J. Phys. Soc. Japan* **59** 4526–33
[26] Baltog I, Baibarac M and Lefrant S 2009 *J.Phys.: Condens. Matter* **21** 025507
[27] Otwinowski Z and Minor W 1997 Processing of x-ray diffraction data collected in oscillation mode *Methods in Enzymology, vol 276: Macromolecular Crystallography, part A* ed C W Carter Jr and R M Sweet (New York: Academic) pp 307–26